# Morphological Aspects of Secondary Crystallization in Poly(ether–ester) Multiblock Copolymers

**R. A. Phillips† and S. L. Cooper*,‡**

*Department of Chemical Engineering, University of Wisconsin–Madison, Madison, Wisconsin 53706*

*Received February 15, 1995; Revised Manuscript Received June 5, 1995®*

ABSTRACT: The morphology of poly(ether–ester) multiblock copolymers with hard segments containing poly(tetramethylene isophthalate) is characterized as a function of the undercooling and hard-segment concentration in isothermal crystallization experiments. At fixed undercooling, the SAXS long spacing increases with decreasing hard-segment concentration and increases strongly with decreased undercooling. Room-temperature storage following crystallization is characterized by a $T_c$-dependent contraction of the long spacing. Similar effects are seen in variable-temperature SAXS thermal contraction experiments, where the decrease in the long spacing on cooling is more rapid at higher $T_c$ for samples of comparable crystallinity. DSC results, and experiments with copolymers containing a mixture of isomers in the hard segments, suggest that both behaviors can be attributed to secondary crystallization on cooling. The observed contraction behavior is qualitatively consistent with models incorporating some form of "morphology control", where the noncrystalline layer thickness is viewed as a contributing factor governing crystallization on cooling. Crystallization of the copolymers is viewed as an extension of the homopolymer crystallization, with additional accounting for fractionation effects and the need to accommodate the soft segment within the semicrystalline microstructure.

## Introduction

The relationship of the solid-state morphology of poly(ether–ester) copolymers to compositional parameters and thermal history has been extensively examined.[1–15] These materials have a multiblock chain architecture with alternating short-chain polyester "hard segments" and polyether "soft segments". The crystallization of the polyester "hard-segment" sequences is an important factor governing the formation of physical cross-links and subsequent mechanical properties. Although the multiblock chain architecture of the copolymers presents complications, analogies with more simple systems are evident. These include (i) semicrystalline blends[16–24] in terms of accommodating a noncrystalline "diluent" within the morphology, (ii) diblock copolymers[25,26] in terms of intrinsic thermodynamic compatibility of the component blocks and the resulting phase behavior, (iii) amorphous-semicrystalline diblock copolymers[27,28] in terms of crystallization with the requirement of chemical connectivity of the noncrystalline component, and (iv) semicrystalline homopolymers with respect to morphology, melting, and reorganization behavior.

Poly(ether–ester) multiblock copolymers with poly(tetramethylene isophthalate) hard segments have been shown to exhibit a reduction in the rate of crystallization and hard-segment melting point.[2,11–13,29–32] Studies of poly(tetramethylene isophthalate)/poly(tetramethylene oxide) (PTMI/PTMO) copolymers have suggested homogeneous melts with respect to microphase separation that extend to temperatures below the hard-segment melting point.[31] Studies of morphology development in these copolymers suggest that microphase separation proceeds in a manner similar to crystallization of the homopolymer, although subtleties exist which are related to changes in the crystal core/surface morphology with changing composition.[32] The multiple melting behavior in these materials has been examined,[11,12,29,31,32] and the structural characterization of the morphologies responsible for the behavior provides an important limiting case for this general class of copolymer architecture. In this study, the effect of isothermal crystallization temperature on the morphology, and subsequent secondary crystallization processes in PTMI/PTMO copolymers, is examined by differential scanning calorimetry (DSC) and small-angle X-ray scattering (SAXS).

## Experimental Section

The poly(ether–ester) copolymers were synthesized using standard procedures[33] from poly(tetramethylene ether) glycol ($M_n$ = 1000) with hard segments based on poly(tetramethylene isophthalate) (PTMI). The sample codes and polymer structure have been discussed and described previously.[31] The compositions of samples used in this study with a single hard-segment type are presented in Table 1. The first number of the sample code corresponds to the weight percentage (nominal value of $W_h$) of the hard segment, and the final ratio corresponds to the ratio of terephthalate (PTMT) to isophthalate (PTMI) in the hard segments. For example, a code of H60/35:65 indicates a copolymer with 60 wt % hard segments whose PTMT/PTMI ratio is 35:65. As in earlier reports,[31,32] $W_h$ is the hard-segment concentration with one hard segment unit formally defined as part of the soft segment, $W_h$* is the total concentration of hard-segments units (the definition applied to this work), and $m$ is the average hard-segment length.

DSC and SAXS experiments utilized samples prepared by compression molding. Prior to molding, the as-received samples were dissolved in HPLC-grade chloroform (Aldrich Chemical Co.), filtered through a 0.5-$\mu$m filter (Millipore), and recovered by film casting. After drying, the films were cut and molded at approximately 25 °C above the as-received melting point for 10 min in a Buehler mount press at 60 MPa. The homopolymer, H100/0:100, could not be dissolved in chloroform and was molded directly from the as-received material. The 2.54-cm-diameter molds were quenched in ice-cooled clamps, and the molded disks were dried for 1 week at room temperature. Samples were subsequently recrystallized in a 2.54-cm-diameter mold without pressure after a 10-min melt treatment to remove residual orientation. Cooling to the crystallization temperature was done by air convection (2–7

* Author to whom correspondence should be addressed.
† Current address: MONTELL Polyolefins, NA Research & Development Center, Elkton, MD 21921.
‡ Current address: College of Engineering, University of Delaware, Newark, DE 19716.
® Abstract published in *Advance ACS Abstracts,* July 15, 1995.

0024-9297/95/2228-5734$09.00/0 

**Table 1. Sample Description**

| sample | $W_h$ | $W_h$* | $m$ |
|---|---|---|---|
| H30/0:100 | 0.29 | 0.433 | 3.1 |
| H60/0:100 | 0.57 | 0.652 | 7.9 |
| H80/0:100 | 0.8 | 0.838 | 22.2 |
| H100/0:100 | 1 | 1 | |

min). Upon cooling to the crystallization temperature, samples were transferred to an air convection oven (Ransco) preset to the crystallization temperature for a period of 6 (H100/0.100), 24 (H80/0:100, H60/0:100), or 48 h (H30/0:100). Samples of H30/0:100 were annealed at the original crystallization temperature for an additional 24 h following the initial crystallization cycle. After crystallization, the molds were quenched in an ice bath, after which the samples were dried under vacuum at room temperature and stored in a desiccator prior to testing.

Differential scanning calorimetry (DSC) was performed using a Perkin-Elmer DSC-7 calorimeter with a Model 7500 series computer station. The DSC was run with liquid nitrogen cooling and a helium purge (15 mL/min, 35 psi) of the sample chambers. Mercury (Aldrich Chemical Co.) and indium (Perkin-Elmer, rod stock) were used as calibrants for temperature and power. Baselines were determined using empty aluminum pans (TA Instruments) in both sample and reference chambers. In all cases the scan rate during heating was 20 °C/min. Samples for DSC were formed from 6−12-mg disks cut from compression-molded samples. Thermal lag was measured by the method of Richardson and Burrington[34] as a function of sample mass and temperature. Results were independent of copolymer composition, and corrections for nonlinearity of temperature scale and absolute lag relative to the dynamic calibration were small and on the order of 0.1−0.6 °C. Enthalpy changes on melting were calculated by integration of the area above the solid to melt baseline by an iterative technique which assumed baseline recovery was governed by the fractional loss in crystallinity. These measurements were used to estimate the weight fraction crystallinity of the freshly quenched samples using a vaue of 121.7 J/g for $\Delta H°$, the enthalpy change on melting of 100% crystalline PTMI.[31] The resultant weight fraction crystallinity was converted to the volume fraction crystallinity, $\phi_c$, assuming crystallites pure in the PTMI component and densities for crystalline and amorphous PTMI of $\varrho_c \sim 1.383 \pm 0.015$ g/cm$^3$ [35] and $\varrho_a = 1.268$ g/cm$^3$ [36] and $\varrho_a = 0.981$ g/cm$^3$ for PTMO.[37]

In SAXS experiments, an Elliot GX-21 rotating-anode generator with copper target, filtered by 25 $\mu$m of nickel foil (A. D. Mackay Inc.), was used as a laboratory source of X-rays ($\lambda = 1.5418$ Å). The generator was operated at or near 40 kV potential and 200 mA emission current. X-rays were collimated by a compact Kratky camera (Anton-Parr). The slit was 7 mm long and 35 $\mu$m in width at the sample. The detector plane was located 26 cm from the source. The flight path was maintained under a vacuum of 3 mmHg. Detection was performed with a Braun OED-50M one-dimensional position-sensitive detector (Innovative Technology) with associated pulse processing electronics. 90/10 argon/methane (Matheson) was used as the flow through counter gas. The standard detector window width of 10 mm was reduced with a home-built mask to approximately 3 mm to reduce the effects of window smearing.[38] The intensity pattern was collected with logic pulse gating on a Tennelec/Nucleus PCAII MCA. Simultaneous measurement of the raw integrated scattering intensity as a function of time was performed with a Canberra Series 35 MCA operated as a multichannel scaler to provide monitoring of source intensity fluctuations. Variable-temperature measurements were performed with hardware designed in-house and utilized sample disks of 2.54 cm diameter.[35] Temperature control to ±1.5 °C was obtained with an Anton-Paar Model K-HR temperature controller. Empty beam scattering was acquired at each of the temperatures for which data were taken. The raw data were corrected for channel-to-channel sensitivity and linearity of the detector. The channel-to-angle conversion was accomplished by a calibration procedure using the three major reflections of cholesterol myristate.[39] The parasitic scattering was subtracted from the empty beam under similar conditions as the data scan after correction of the data for angular-dependent transmittance, counting time, intensity fluctuations, polarization, and dead-time. Intensities were converted to an absolute scale by calibration against a standard Lupolen sample. Desmearing was accomplished with the method of Lake[40] using an experimentally determined slit-length weighting function of the primary beam corrected for the finite detector window width. Application of the expression by Ruland[41] to the high angle data was made for subtraction of the thermal density fluctuation contribution to the scattering prior to analysis.

Room temperature SAXS patterns were collected after extended periods of storage (>2 months) and after freshly quenching from the crystallization temperature. After 10 min at room temperature, patterns of the freshly quenched materials were collected for 60 min. A similar protocol was followed in the thermal contraction experiments. A pattern was collected for 1 h at a temperature below $T_c$ (allowing for 10 min of stabilization) following pretreatment (10 min) at 5 °C below the original $T_c$. Lorentz-corrected SAXS long spacings, $L$, were calculated according to eq 1. In eq 1, $q^*$ is the

$$L = 2\pi/q^* \tag{1}$$

scattering vector magnitude ($q = 4\pi \sin(\theta)/\lambda$) at the maximum value of $q^2I$, where $I$ is the desmeared scattering intensity, $\theta$ is half the scattering angle, and $\lambda$ is the X-ray wavelength. An approximate estimate of the characteristic crystalline and amorphous domain sizes is made by application of a parallel stack model, where the long spacing is given by the sum of crystalline ($\langle l\rangle_c$) and amorphous ($\langle l\rangle_a$) layer thicknesses. Values of $\langle l\rangle_c$ are calculated according to eq 2. Analysis of the 1D

$$\langle l\rangle_c = \phi_c L \tag{2}$$

correlation function gave alternative values for the crystalline thickness, $\langle l\rangle_{c,1D}$, and long spacing, $L_{1D}$. The correlation functions are calculated according to eq 3. $L_{1D}$ was calculated

$$\gamma(x) = \frac{\int_0^\infty q^2 I(q) \cos(qx)\, dq}{\int_0^\infty q^2 I(q)\, dq} \tag{3}$$

from the first maxima in the correlation function, and $\langle l\rangle_{c,1D}$ was calculated according to eq 4. In eq 4, $x_0$ is the value of

$$\langle l\rangle_{c,1D} = x_0/(1 - \phi_c) \tag{4}$$

the correlation distance where the line describing the tangent at maximum slope to $\gamma(x)$ is zero.[42,43] The experimental estimates of $\phi_c$ from DSC were used in eq 4, although numerical values of $\langle l\rangle_{c,1D}$ showed only minor differences from direct evaluation of the correlation triangle construction.[42,43] Interpretation of the SAXS data in terms of one-dimensional models is consistent with a lamellarlike organization in the poly(ether−ester) copolymers.[1,2,6-8]

## Results

**SAXS Studies of Undercooling Dependence.** Figure 1 shows representative SAXS patterns, collected at room temperature, of H30/0:100, H60/0:100, H80/0:100, and H100/0:100 freshly quenched from the isothermal crystallization temperature. Figure 2 shows representative effects of the crystallization temperature on the room-temperature SAXS patterns for freshly quenched samples of H60/0:100. The Lorentz-corrected SAXS long spacing $L$, calculated according to eq 1, is shown as a function of composition and undercooling ($\Delta T$) in Figure 3. Values of the undercooling, $\Delta T$, are based on equilibrium melting points for each composition that have been estimated elsewhere.[31,35] The decrease in $L$ with increasing $\Delta T$ observed in Figure 3 for H30/0:100 is not

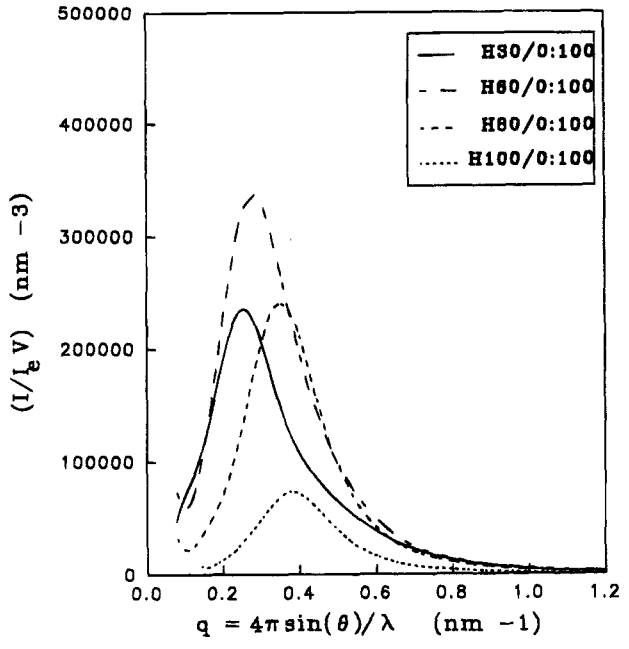


**Figure 1.** SAXS patterns of H30/0:100, H60/0:100, H80/0:100, and H100/0:100 collected at room temperature after crystallization at an undercooling, $\Delta T$, of approximately 50 °C. Samples were freshly quenched (60-min collection from the crystallization temperature.

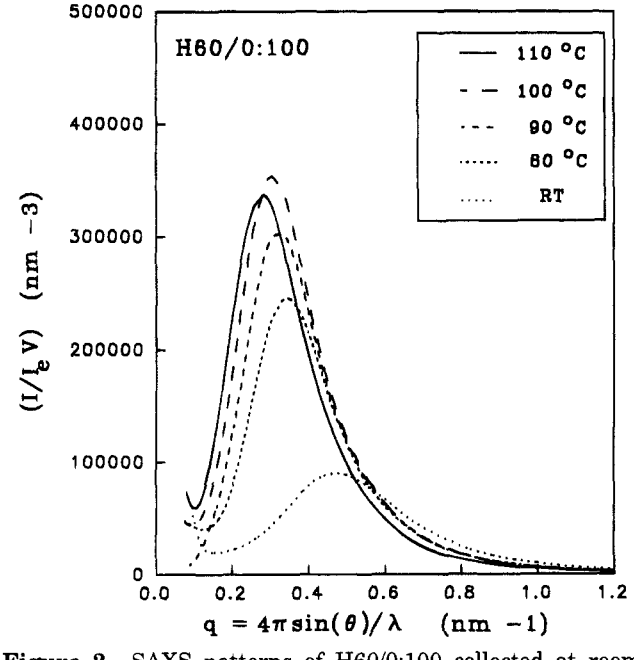


**Figure 2.** SAXS patterns of H60/0:100 collected at room temperature after crystallization at the indicated temperatures. Samples were freshly quenched (60 min collection) from the crystallization temperature.

observed in the raw intensity maxima (without $q^2$-weighting). This decrease is due to the sensitivity of the peak shape of H30/0:100 to the Lorentz correction. For undercoolings less than the undercooling of the maximum crystallization rate ($\Delta T$ < 80 °C), the long spacing data are adequately represented by a proportionality to the inverse undercooling as shown in Figure 4. Using the correlation of Figure 4, the relationship of the long spacing to the bulk composition is approximately linear, as illustrated in Figure 5. The extension of this correlation to H30/0:100 is made with the qualification noted above.

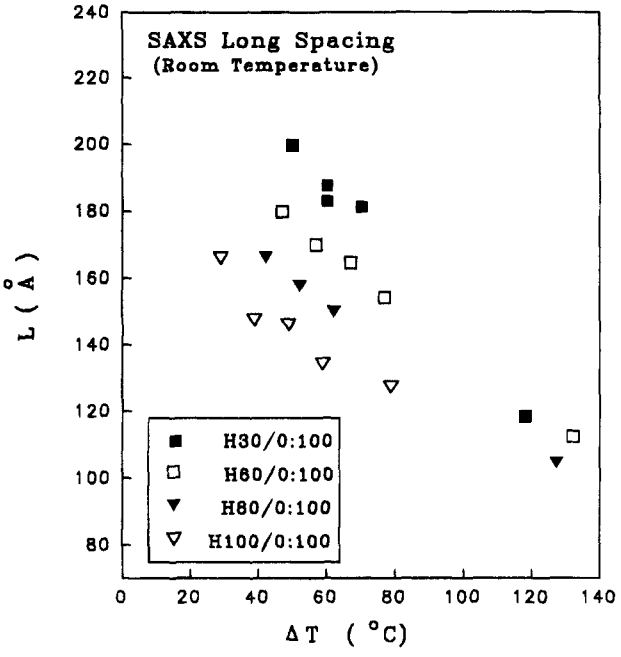


**Figure 3.** Lorentz-corrected SAXS long spacing, $L$, from patterns of H30/0:100, H60/0:100, H80/0:100, and H100/0:100 collected at room temperature after crystallization at the indicated undercoolings. Samples were freshly quenched (60-min collection) from the crystallization temperature.

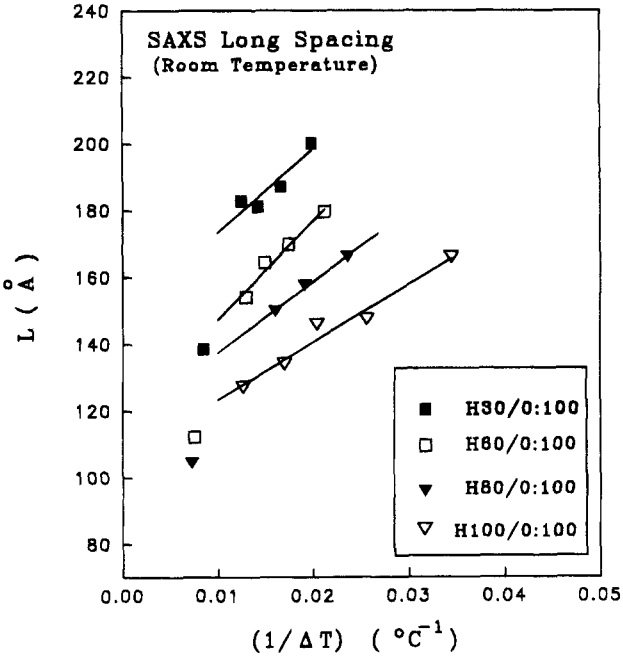


**Figure 4.** Dependence of Lorentz-corrected SAXS long spacing, $L$, on the inverse undercooling, $\Delta T^{-1}$, evaluated from patterns of H30/0:100, H60/0:100, H80/0:100, and H100/0:100 collected at room temperature. Samples were freshly quenched (60-min collection) from the crystallization temperature.

Values of $L$, $\langle l \rangle_c$, $L_{1D}$, and $\langle l \rangle_{c,1D}$ are summarized in Table 2. A representative set of 1D correlation functions is shown in Figure 6. These correlation functions correspond to the SAXS intensity patterns shown in Figure 1. Generally, at higher hard-segment content, values of the long spacing and crystalline layer thickness calculated from $\gamma(x)$ are lower than the corresponding values obtained by direct interpretation of the SAXS intensity maxima. This tendency is observed for other semicrystalline polymers.[44,45] In some cases, this discrepancy has been interpreted as owing to the polydis-

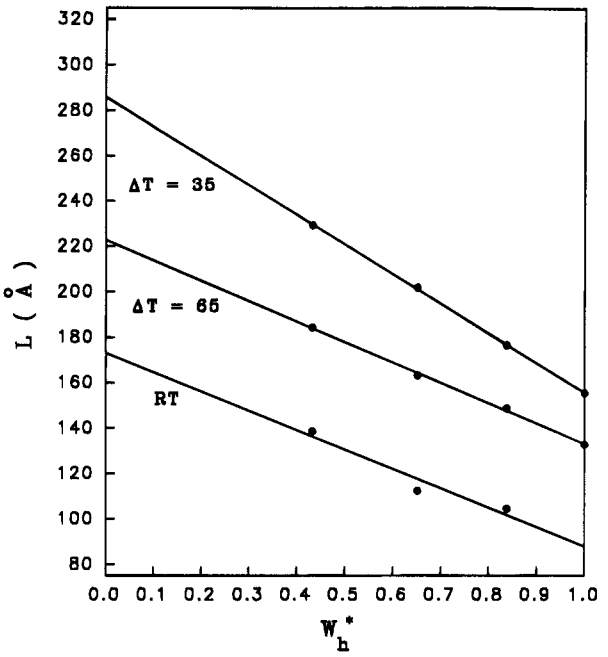


**Figure 5.** Dependence of the Lorentz-corrected SAXS long spacing on the bulk composition for patterns collected at room temperature. The data apply to samples freshly quenched (60-min collection) from the crystallization temperature.

**Table 2. SAXS Morphology Characterization**[a]

| $\Delta T$ (°C) | $\phi_c$ | $L$ (Å) | $\langle l \rangle_c$ (Å) | $L_{1D}$ (Å) | $\langle l \rangle_{c,1D}$ (Å) |
|---|---|---|---|---|---|
| | | H100/0:100 | | | |
| 29 | 0.314 | 165.9 | 52.0 | 159.4 | 41.8 |
| 39 | 0.321 | 147.4 | 47.3 | 136.4 | 40.1 |
| 49 | 0.331 | 145.9 | 48.3 | 139.1 | 37.8 |
| 59 | 0.350 | 134.1 | 46.9 | 127.8 | 35.9 |
| 79 | 0.294 | 127.2 | 32.8 | 119.8 | 30.9 |
| | | H80/0:100 | | | |
| 42 | 0.292 | 166.0 | 48.4 | 157.1 | 36.8 |
| 52 | 0.303 | 157.6 | 47.8 | 149.0 | 36.7 |
| 62 | 0.310 | 149.8 | 46.4 | 140.3 | 34.0 |
| 137 | 0.181 | 104.4 | 18.9 | 97.9 | 21.4 |
| | | H60/0:100 | | | |
| 47 | 0.211 | 179.6 | 37.8 | 177.4 | 33.7 |
| 57 | 0.208 | 169.8 | 35.3 | 165.4 | 31.9 |
| 67 | 0.217 | 164.4 | 35.6 | 159.9 | 30.8 |
| 77 | 0.221 | 154.1 | 34.0 | 144.5 | 28.8 |
| 132 | 0.182 | 112.2 | 20.4 | 104.6 | 22.2 |
| | | H30/0:100 | | | |
| 50 | 0.048 | 200.1 | 9.6 | 209.0 | 23.2 |
| 60 | 0.076 | 187.2 | 14.2 | 191.2 | 23.1 |
| 70 | 0.090 | 181.1 | 16.3 | | 24.9 |
| 80 | 0.080 | 182.8 | 14.6 | | 25.4 |
| 118 | 0.100 | 138.5 | 13.9 | 152.9 | 24.0 |

[a] Volume fraction crystallinity estimates were made from DSC measurements, $L$ was calculated by eq 1, $\langle l \rangle_c$ was calculated by eq 2, and $L_{1D}$ and $\langle l \rangle_{c,1D}$ were calculated from 1D correlation function constructions (eqs 3 and 4). Missing values of $L_{1D}$ for H30/0:100 were due to a very broad first maximum in the correlation function.

persity in the distribution of long spacings.[44,45] Regardless of the calculation method, the long spacing is observed to decrease with increased undercooling and increasing hard-segment content. These long spacing variations appear dominated by the amorphous layers. Changes in the crystalline layer thickness with respect to undercooling are comparatively much smaller but decrease with decreasing hard-segment content.

**Secondary Crystallization on Storage.** Figures 7–9 show the DSC scans of H30/0:100, H60/0:100, and H80/0:100 following crystallization at elevated temperature and subsequent storage at room temperature.

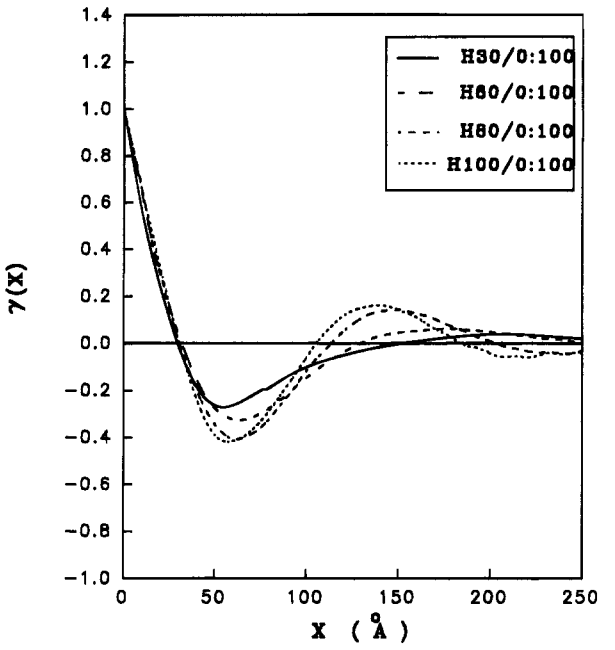


**Figure 6.** One-dimensional correlation functions of H30/0:100, H60/0:100, H80/0:100, and H100/0:100 from SAXS patterns collected at room temperature after crystallization at an undercooling, $\Delta T$, of approximately 50 °C. The correlation functions correspond to the patterns shown in Figure 1.

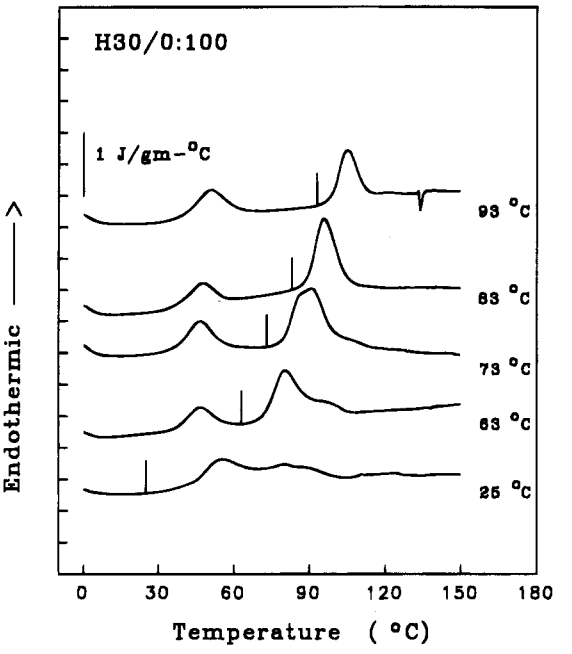


**Figure 7.** DSC scans taken after room-temperature aging of H30/0:100. Small vertical lines indicate the original isothermal crystallization prior to room-temperature aging.

Previous investigations of the melting behavior after isothermal crystallization (without room-temperature storage) have previously been published.[31,32] The significant difference observed here compared to previous results is the thermal event which occurs at temperatures below the original crystallization temperature. In the DSC scans of samples aged at room temperature, the peak position of this feature is about 50 °C and increases in magnitude and position during storage. This apparent endotherm is particularly prominent in the softer copolymers.

Figure 10 shows the results of annealing (15 min) at 40, 50, 70, and 95 °C for a sample of H60/0:100 which was initially prepared by isothermal crystallization at

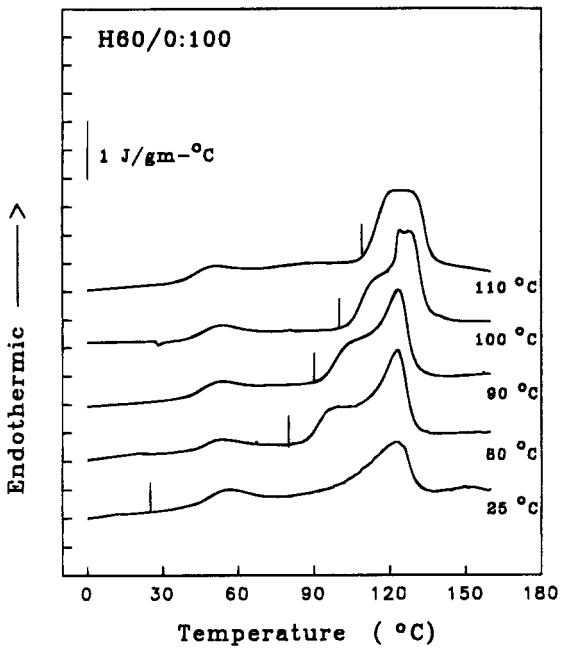


**Figure 8.** DSC scans taken after room-temperature aging of H60/0:100. Small vertical lines indicate the original isothermal crystallization prior to room-temperature aging.

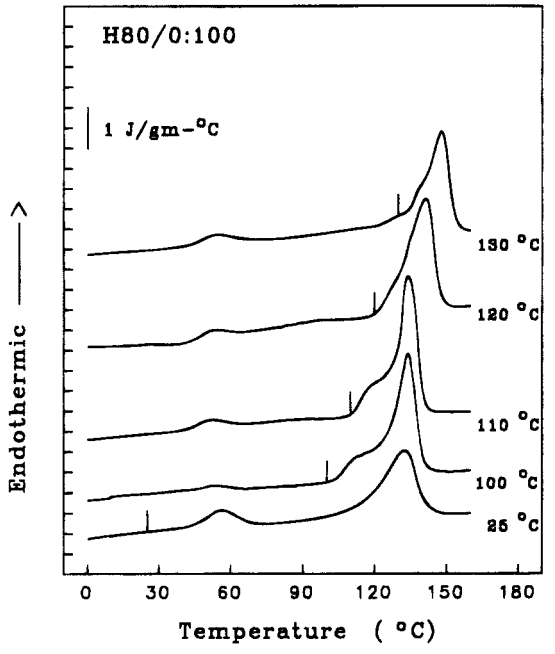


**Figure 9.** DSC scans taken after room-temperature aging of H80/0:100. Small vertical lines indicate the original isothermal crystallization prior to room-temperature aging.

110 °C and subsequently stored at room temperature. The aged sample (Figure 8) shows a broad range of apparent ordering at temperatures below the original crystallization temperature. Even for very low annealing temperatures, the initial thermal event has been shifted to higher temperature, with the original $T_g$-like character not recovered on rescanning.

The nature of the room-temperature aging process is further illustrated by crystallization and annealing experiments of copolymers containing both PTMT and PTMI in the hard segments. These materials exhibit a large reduction of the melting point, the crystallization rate, and a prominent low-temperature endotherm which develops during room-temperature crystallization.[11,29,35] Minimal melting is observed at tempera-

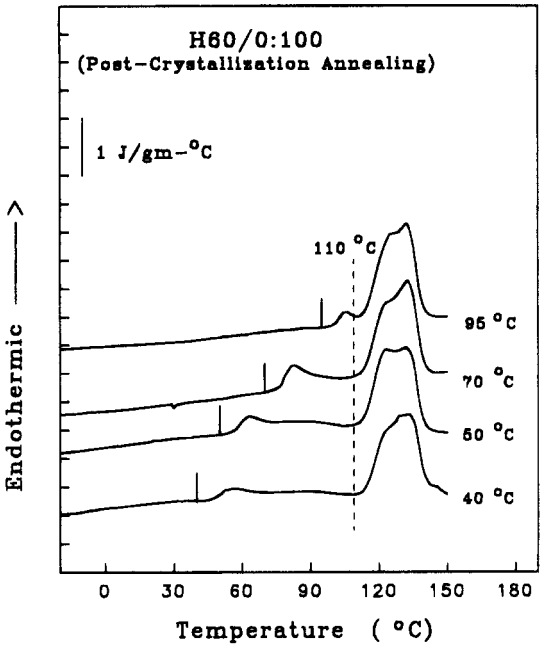


**Figure 10.** DSC scans of H60/0:100 after annealing at the indicated temperatures (solid vertical lines) for 15 min. Prior to annealing, the sample was formed by isothermal crystallization at 110 °C (vertical dashed line) and subsequently allowed to age at room temperature.

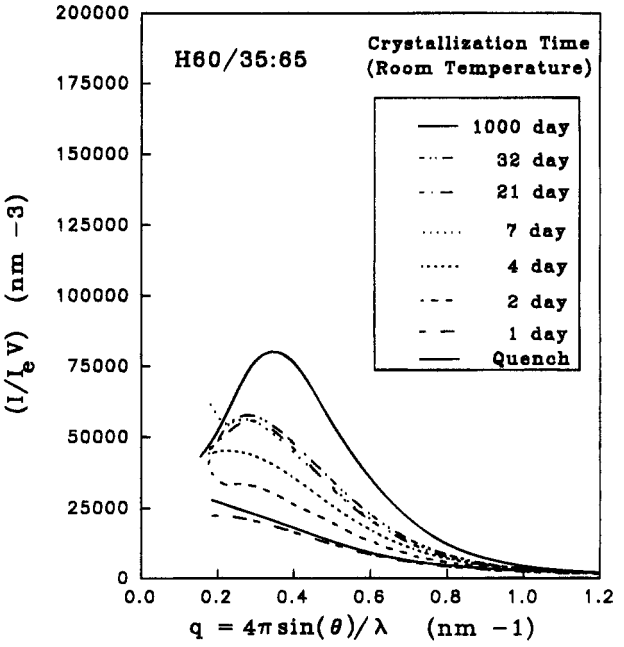


**Figure 11.** SAXS pattern development from H60/35:65 during isothermal crystallization from the melt at room temperature. H60/35:65 is analogous to H60/0:100 in bulk composition, but with a mixture of PTMT/PTMI in the ratio 35:65.

tures above this endotherm when crystallization is allowed to occur at room temperature due to the reduction in sequence length of the hard-segment component which is crystallizable. The position of this endotherm is similar to that associated with the lower temperature melting of the aged samples shown in Figures 7–9. This can be seen during the structure development of H60/35:65. Crystallization was monitored over the course of 32 days and finally much later after approximately 1000 days. The SAXS profile development is shown in Figure 11, and the corresponding DSC scans are shown in Figure 12. After the longest time studied, a well-defined long spacing of 128

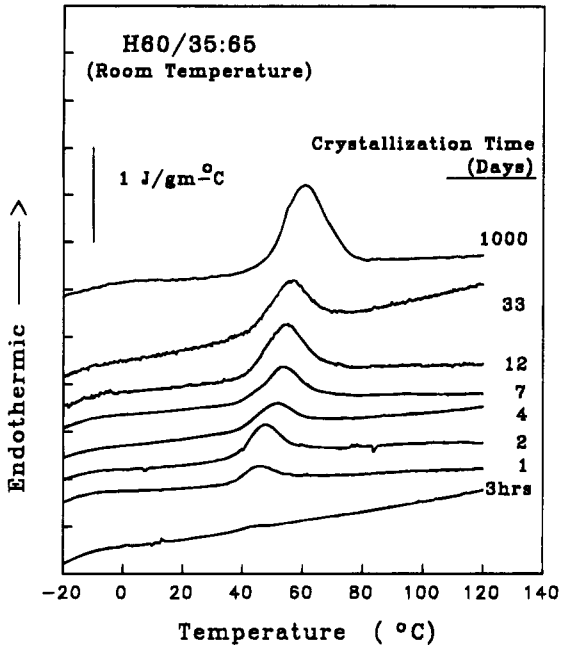


**Figure 12.** DSC scans of H60/35:65 during isothermal crystallization from the melt at room temperature. H60/35:65 is analogous to H60/0:100 in bulk composition, but with a mixture of PTMT/PTMI in the ratio 35:65.

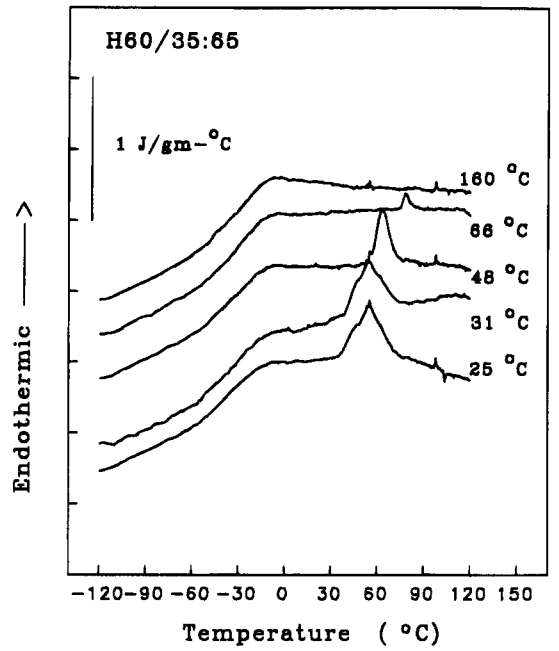


**Figure 13.** DSC scans of H60/35:65 following annealing (15 min) at the indicated temperatures. The starting sample was formed by isothermal crystallization from the melt at room temperature. H60/35:65 is analogous to H60/0:100 in bulk composition, but with a mixture of PTMT/PTMI in the ratio 35:65.

Å has developed. Figures 13 and 14 show the DSC scans after annealing samples of H60/35:65 and H80/33:67 for 15 min at the indicated temperatures. Both of these samples were prepared by crystallization at room temperature prior to the annealing treatments. Despite the low crystallinity in these materials, all are partially opaque and become clear on heating, indicating the endotherm is associated with crystalline ordering. The rescans following annealing treatments show only a single glass transition temperature.

**SAXS Studies of Secondary Crystallization on Cooling.** Figure 15 shows the effect of room-temperature aging on the SAXS long spacing in H60/0:100. Representative SAXS patterns illustrating the storage effect are shown in Figure 16 when the initial crystallization temperature is 110 °C. The inset to Figure 16 shows the corresponding 1D correlation functions. The comparison of patterns for the freshly quenched and aged samples shows that the scattering peak changes shape on storage, broadening toward higher $q$-values with a *decrease* in peak intensity. These results suggest a contraction in the long spacing during room-temper-

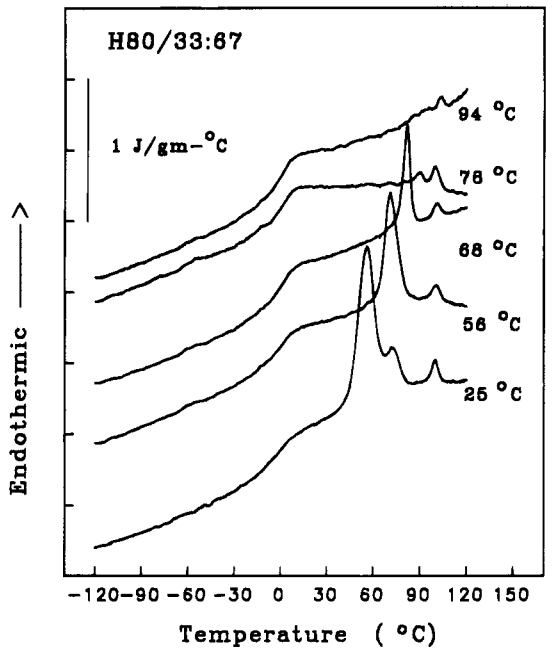


**Figure 14.** DSC scans of H80/33:67 following annealing (15 min) at the indicated temperatures. The starting sample was formed by isothermal crystallization from the melt at room temperature. H80/33:67 is analogous to H80/0:100 in bulk comparison, but with a mixture of PTMT/PTMI in the ratio 33:67.

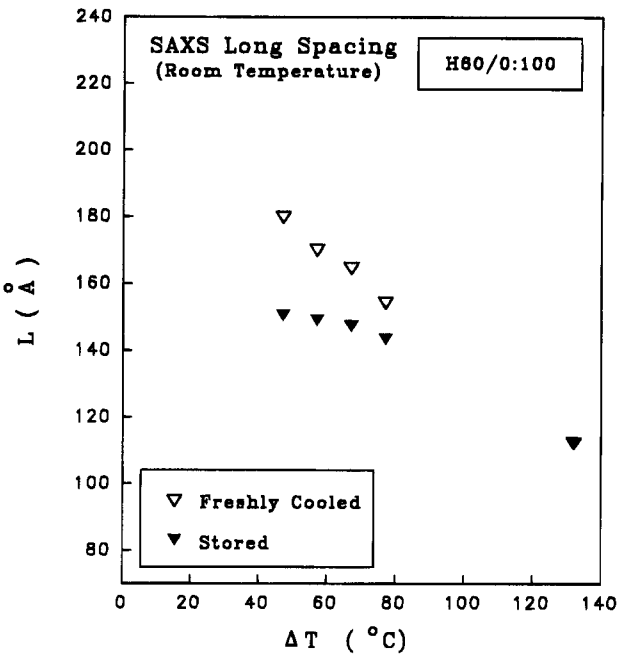


**Figure 15.** Lorentz-corrected SAXS long spacing, $L$, vs undercooling, $\Delta T$, from patterns of H60/0:100 collected at room temperature. Data are presented for samples freshly quenched (60-min collection) from the crystallization temperature and for samples aged at room temperature with the same initial undercooling as the freshly quenched samples.

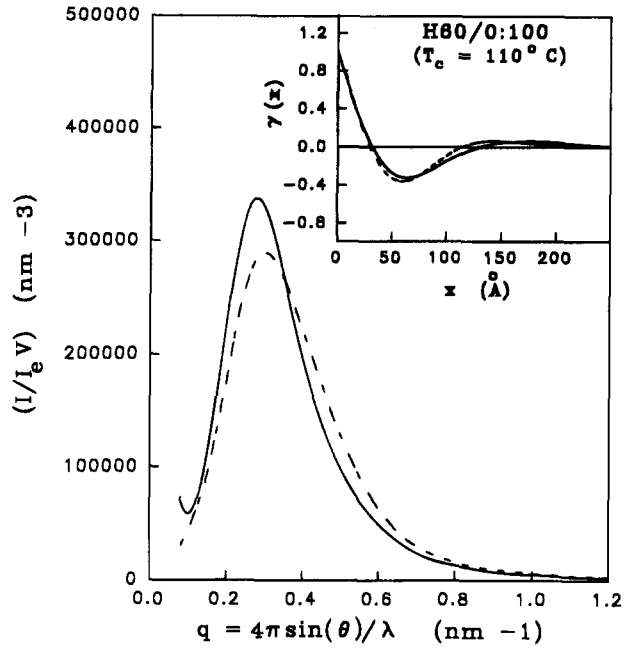


**Figure 16.** SAXS patterns of H60/0:100 collected at room temperature following crystallization at 110 °C ($\Delta T = 47$ °C). Data are presented for samples freshly quenched (60-min collection, solid line) from the crystallization temperature and for samples aged at room temperature with the same initial undercooling as the freshly quenched sample (dashed line). The inset shows the corresponding one-dimensional correlation functions.

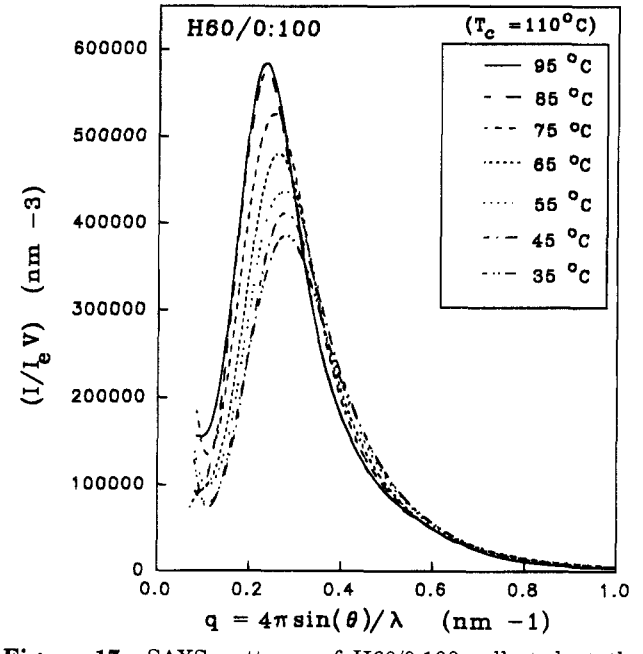


**Figure 17.** SAXS patterns of H60/0:100 collected at the indicated temperatures after cooling from the original crystallization temperature of 110 °C. Data collection (60 min) at each temperature was preceded by a 10-min treatment at 5 °C below the initial $T_c$.

ature storage which is dependent on the starting morphology. The morphology dependence is evidenced by the increased contraction of the long spacing ($\Delta L = L_0 - L$) as the initial long spacing, $L_0$, is increased.

Figures 17 and 18 show representative SAXS patterns of H60/0:100 during cooling from the crystallization temperature 110 and 80 °C, respectively). The SAXS patterns show a contraction of the long spacing on cooling. This is expected due to the effect of thermal expansion. On cooling from the crystallization temperature, the density of the respective domains is expected to increase (thermal contraction), resulting in a net volume contraction and decreasing periodicity.

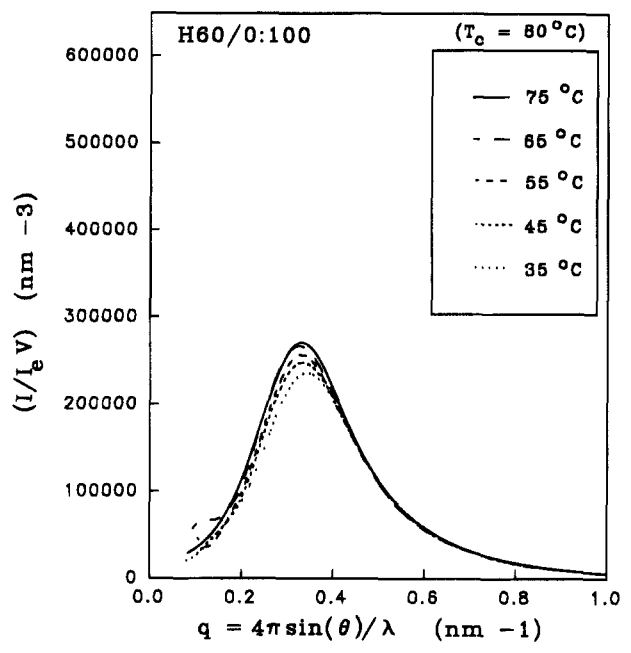


**Figure 18.** SAXS patterns of H60/0:100 collected at the indicated temperatures after cooling from the original crystallization temperature of 80 °C. Data collection (60 min) at each temperature was preceded by a 10-min treatment at 5 °C below the initial $T_c$.

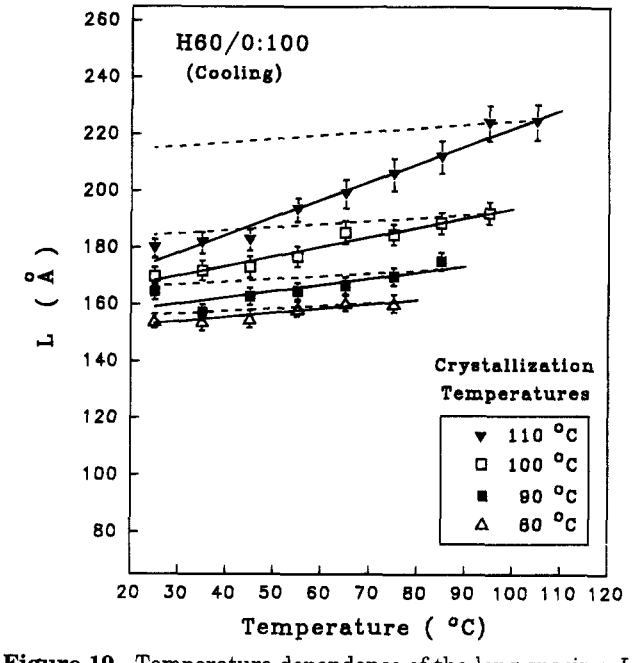


**Figure 19.** Temperature dependence of the long spacing, $L$, after cooling from the original crystallization temperature. Data collection (60 min) at each temperature was preceded by a 10-min treatment at 5 °C below the initial $T_c$. The dashed lines represent the predicted changes due solely to thermal contraction, drawn from the experimental value of $L$ at 5 °C below $T_c$.

Figure 19 shows the long spacing data on cooling. The dashed lines in Figure 19 illustrate the predicted decrease in the long spacing, using the thermal expansion coefficients for crystalline and amorphous PTMT quoted by Fakirov et al.[46] ($\alpha_c = 5.4 \times 10^{-4}$ g/cm$^3$·K, $\alpha_h = 7.7 \times 10^{-4}$ g/cm$^3$·K) and literature reports for liquid PTMO[37] ($6.84 \times 10^{-4}$ g/cm$^3$·K). Due to the uncertainty

in these parameters, applied to the current system (with PTMI hard segments), these predictions are only qualitative and illustrate the expected decrease of the long spacing on cooling. Little sensitivity to the original crystallization temperature is predicted due to similar initial crystallinities (thermal contraction governed by crystallinity). For lower initial crystallization temperatures, the predicted change in $L$ due to thermal contraction is adequately approximated. However, the decrease in $L$ on cooling is morphology dependent. The long spacing contracts more rapidly with higher initial $T_c$. In this sense, secondary crystallization on cooling from elevated crystallization temperatures has an analogous effect as the room-temperature aging results shown previously in Figures 15 and 16.

## Discussion

The increase in long spacing with decreasing hard-segment concentration (Figures 3−5) is consistent with related studies on PTMT/PTMO systems.[6,46] Other literature reports of PTMT/PTMO copolymers annealed in the solid state suggest a weak composition dependence.[6,7] In this work, the samples were prepared by isothermal crystallization. At low undercooling, the composition dependence of the long spacing is consistent with decreasing crystallinity and increasing specific volume of the amorphous regions as the hard-segment concentration is decreased.[46] Table 2 suggests that the dominant contribution to the long spacing changes with undercooling is attributable to the amorphous layer thickness, with a smaller variation in $\langle l \rangle_c$.

For the materials freshly quenched following isothermal crystallization at low undercooling (with room-temperature data collection), the data in Table 2 suggest that "high-end" estimates of the crystalline layer thickness imply approximately 4 repeat units in H100/0:100 and H80/0:100, 3−4 units in H60/0:100, and 1−2 units in H30/0:100. This assumes the same $c$-axis crystalline repeat distance as in PTMT (11.7 Å).[47,48] An additional assumption is that of lamellar morphologies, which may not be applicable in H30/0:100. The results summarized in Table 2 indicate that the estimates for $\langle l \rangle_c$ are much less than the average hard-segment length (see Table 1), irrespective of undercooling. Bandara and Dröscher[7] presented room-temperature SAXS patterns of poly(ether−ester) copolymers with PTMT hard segments after solid-state annealing. Values of $\langle l \rangle_c$ from 1D correlation function calculations, as well as values calculated from direct application of the long spacing, showed a weak dependence on undercooling. Large deviations between correlation function calculations and long spacing calculations were observed at low hard-segment concentration. The results presented here for PTMI containing poly(ether−ester) copolymers, which crystallize at a much slower rate,[11,29,31,32,35] are similar. This suggests that the crystallization rate is a relatively weak factor governing the lamellar morphology in poly(ether−ester) copolymers. The dominant factors are the undercooling and the hard-segment concentration/composition.

Figures 7−9 show that, during room-temperature storage, a prominent endotherm develops with a peak transition temperature of about 50 °C. The endotherm is generally more prominent as the hard-segment concentration, and crystallinity prior to storage, decreases. Even for very low annealing temperatures following storage (Figure 10), the initial low-temperature thermal transition has been moved to higher temperature. The original $T_g$-like character of the transition is not recovered on rescanning. This indicates that, if the initial event was a glass transition, it is unstable to recrystallization and/or mixes with the amorphous regions after a small elevation in temperature. The latter explanation is shown at the higher annealing temperatures where recrystallization is slowed and no evidence of the initial thermal event is recovered after cooling. Similar effects are seen in the annealing experiments of mixed hard-segment copolymers shown in Figures 13 and 14. In addition, the peak temperature of the endotherm which develops during room-temperature storage for the copolymers is approximately 10 °C higher than the enthalpy relaxation maxima previously observed in the homopolymer.[31,35] This indicates that the thermal event in the copolymers has different origins than the glass transition of the homopolymer.

The low-temperature annealing endotherm is particularly prevalent in the copolymers containing a mixture of hard-segment isomers (Figures 12−14). These mixed isomer materials are all partially opaque and become clear on heating, indicating that the low-temperature endotherm is associated with crystalline ordering. The rescans following annealing shown in Figures 13 and 14 give no evidence for an apparent hard-segment $T_g$. This suggests that segmental mixing occurs following melting at these relatively low temperatures. Previous work on PTMI/PTMO multiblock copolymers has suggested homogeneous melts with respect to microphase separation that extend to temperatures below the hard-segment melting point.[31] The low melting point, and short average length of the crystallizable species in materials with a mixture of hard-segment isomers,[11,29] is suggestive of small size and/or disorder of the structures which develop. This result suggests an analogy with the morphological observations associated with the lower temperature melting/ordering which develops during room-temperature aging of copolymers with a single hard-segment type. In agreement with previous results,[29] Figures 11 and 12 suggest that the increase of SAXS intensity roughly coincides with the evolution of the DSC melting endotherm, supporting the hypothesis of hard-segment ordering associated with the room-temperature annealing endotherm. Stevenson[13,29] has observed similar results and provided evidence that mechanical property evolution in these materials also coincides with the evolution of the crystalline fraction.

During room-temperature storage in the PTMI/PTMO copolymers, the SAXS patterns shown in Figure 16 illustrate that the scattering maximum changes shape on storage, broadening toward higher $q$-values. The crystallization which occurs during storage also results in a *decrease* in peak intensity. This suggests that the scattering behavior is not solely due to the addition of an independent structure of smaller periodicity (which from Figure 11 is known to occur) but rather is the result of a modification *within* the existing structure. This modification gives rise to a net contraction of the long spacing. The magnitude of the contraction is a clear function of the starting morphology, as shown in Figure 15, with a larger contraction observed as the initial long spacing increases.

The SAXS thermal contraction experiments shown in Figures 17 and 18 provide additional insight into the morphological aspects of the secondary crystallization process during cooling. The morphology-dependent contraction of the SAXS long spacing shown in Figure

19 is not expected based solely on thermal contraction/expansion considerations. Similar departures from thermal expansion have been shown in the intensity invariant.[35] Scanning SAXS experiments by Fakirov et al.[46] also showed departures in anticipated thermal expansion behavior in poly(ether–ester) copolymers with PTMT hard segments and poly(ethylene oxide) (PEO) soft segments. This was explained by two factors: (i) a reversible melting/crystallization of imperfect crystallites within the existing crystalline structure (a view supported here) or (ii) demixing in the amorphous regions on heating.

As discussed, the departures observed here are associated with a secondary crystallization process. This viewpoint is supported by previous studies[32] which indicate that microphase separation in these copolymers is dominated by the crystallization process. Furthermore, only small variations in $T_g$ are observed with postcrystallization annealing treatments. The secondary crystallization which occurs from within the existing structure influences the SAXS patterns on cooling. The long spacing contracts more rapidly with higher initial $T_c$ because secondary crystallization has a larger effect within the larger amorphous regions at high $T_c$. In this sense, secondary crystallization following cooling at elevated temperature is conceptually analogous to the effects of initial undercooling and composition during room-temperature aging.

**Secondary Crystallization Effects: Model Considerations.** Previous work has suggested the importance of fractionation by hard-segment length during the crystallization of poly(ether–ester) copolymers with PTMT sequences.[9,10] This process was proposed to occur by a coupling of the hard-segment length distribution with the stable crystallite size at the crystallization temperature ($T_c$). Descriptively, this would result in the exclusion of shorter sequence lengths at higher temperatures due to a larger core crystal size. The qualitative observation of proportionally larger low-temperature endotherm development during room-temperature aging in the softer copolymers, and copolymers with a mixture of hard-segment isomers (Figures 6–9 and 12 and ref 11, 29, and 35), appears consistent with this conjecture. That is, the small size/disorder of structures which are associated with the lower temperature melting (Figure 11) can accommodate very short runs of crystallizable sequences that would not be stable at elevated crystallization temperatures. In this way, the crystallization of shorter sequences on cooling may contribute to thermal contraction and room-temperature aging effects.

An additional consequence of hard-segment fractionation would be a reduction in the degree of crystallinity with increasing $T_c$. Limiting values of the DSC-measured heat of fusion, $\Delta H$, following isothermal crystallization are estimated in Figure 20 for all compositions. H80/0:100 shows behavior similar to that of the homopolymer. As the undercooling decreases, the limiting crystallinity actually increases slightly. In H60/0:100 the plateau value of $\Delta H$ is relatively constant over the range of crystallization temperatures. For the softest copolymer studied (H30/0:100), the ultimate degree of crystallinity is strongly temperature dependent, decreasing with decreased undercooling. This suggests, as alluded to earlier, that fractionation effects may become an important factor controlling the extent of crystallization in H30/0:100 at experimentally accessible undercoolings. The high-end estimates of $\langle l \rangle_c$ indicate that sequences less than 3 units long in H80/0:100 and 2–3 units long in H60/0:100 are excluded at lower undercooling and may become incorporated into crystallites on cooling to room temperature.

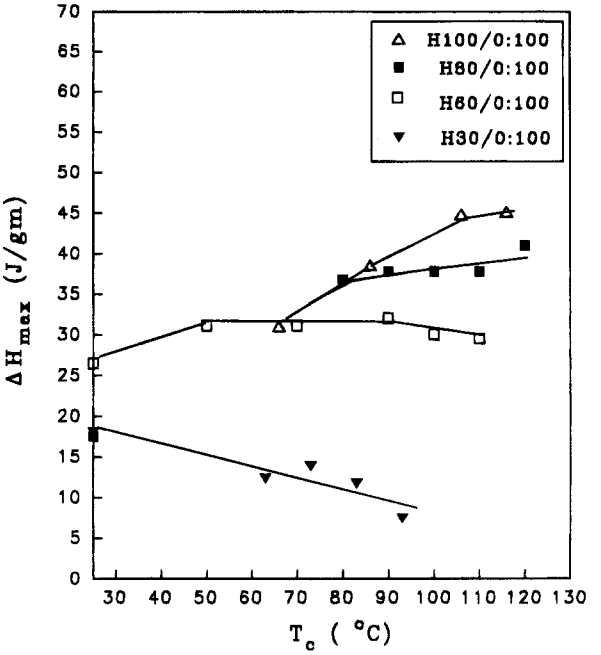


**Figure 20.** Estimates of the "limiting" value of $\Delta H$ determined from DSC data at long crystallization times. The values for H30/0:100 are taken from the magnitude of the higher temperature endotherms in Figure 7 (72 h). For H60/0:100, H80/0:100, and H100/0:100 average values at later times are taken (18–24 h in H80/0:100, 2–3 h in H100/0:100, and from Figure 8 for H60/0:100).

With the possible exception of very low undercoolings in H60/0:100, it does not appear at higher hard segment concentrations that the degree of crystallinity is controlled by depletion of hard segments of lengths compatible with the core crystal size. This latter conclusion is supported by degree of crystallinity estimates. In the extreme fractionation limit, if all of the sequences of length $\zeta$ or greater crystallize, the degree of crystallinity can be predicted for a minimum sequence length, $\zeta_{min}$. Assuming a most probable distribution of hard-segment lengths and approximate values for $\zeta_{min}$ of 3–4 units and 4 units in H60/0:100 and H80/0:100, predicted degrees of crystallinity for H60/0:100 and H80/0:100 are approximately 0.52–0.55 and 0.79, respectively. The predicted crystallinities require crystallization of identical sequence lengths, which, athough an unphysical limit, provides an upper bound. These calculated values overpredict the observed crystallinities which are approximately 0.25 and 0.32. This does not suggest that fractionation is not active, as discussed earlier, but only that other factors such as kinetic effects, and cocrystallization of disparate sequence lengths, control the ultimate extent of crystallization at higher hard-segment content. As discussed by Briber and Thomas,[9,10] the latter effect would be expected to create an intrinsically irregular interfacial structure, which has been suggested by indirect thermal measurements.[32]

A "postcrystallization" endotherm positioned slightly above the annealing temperature is not unique to copolymer systems.[12,49–52] In this sense, although sequence length effects play a role, secondary crystallization effects in the poly(ether–ester) copolymers do not require a strict reliance on sequence length fractionation. The model of Strobl et al.[42,53] based on SAXS and

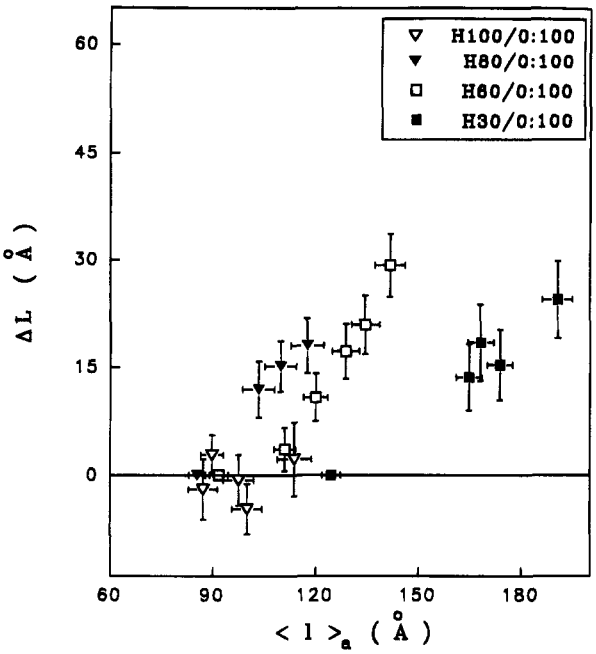


**Figure 21.** Magnitude of the long spacing contraction resulting from room-temperature aging. $\Delta L$ is the difference of the long spacing from samples freshly quenched from the original $T_c$ (60-min collection) and the long spacing after room-temperature storage ($\Delta L = L_{cooled} - L_{stored}$). $\langle l \rangle_a$ is the calculated amorphous layer thickness ($\langle l \rangle_a \sim L - \langle l \rangle_c$) of the freshly quenched samples. Variations in $\langle l \rangle_a$ were obtained by altering the initial undercooling and bulk composition. The first nonzero point for H60/0:100 applies to a sample annealed in the solid state (as compared to isothermal crystallization) at 90 °C prior to storage. The points at zero contraction for H80/0:100, H60/0:100, and H30/0:100 represent the molded material crystallized at room temperature.

microscopy investigations of low-density polyethylene seems able to describe many of the relevant experimental observations in the present work. In this model, crystallization on cooling is governed by the interlamellar space (amorphous layer spacings) available for crystallization. This model suggests that the crystal thickness is controlled by the crystallization temperature, and the formation of new lamellae can occur between preexisting lamellae only if space is available for the stable crystal thickness. As the temperature is further lowered, thinner lamellae are able to form, resulting in continued contraction of the observed long spacing. In this way, it was proposed that each lamellae has a "memory" of the temperature at which it was formed, with the dominant factor governing crystallization on cooling attributed to the temperature-dependent stability limits for the amorphous layers. Other mechanisms have been proposed with varying degrees of similarity by other investigators.[50,54–57]

Figure 21 illustrates the relationship between the magnitude of the long spacing contraction following room-temperature storage with estimates of the amorphous layer thickness immediately after quenching. The absolute magnitude of the $\langle l \rangle_a$ values in H30/0:100 may be somewhat overestimated due to the simplified calculation procedure. Nevertheless, at fixed hard-segment concentration, all materials show a continuous decrease in the observed contraction with decreasing $\langle l \rangle_a$. The variation of $\langle l \rangle_a$ was achieved by varying the initial undercooling. Similarly, the cooling experiments associated with Figures 17–19 also suggest larger long spacing contraction effects at lower initial undercoolings, resulting in morphology-dependent thermal expansion/contraction effects. Magill et al.[58] reported similar $T_c$-dependent contractions of the long period in poly(tetramethylphenylenesiloxane). Temperature-dependent changes in the amorphous layer on cooling were postulated to describe these effects in a manner somewhat analogous to the "premelting" concept of Fischer.[59,60] In this viewpoint, the morphology of the amorphous layers changes reversibly with temperature, although the mechanism by which this is brought about is to some extent unclear. In the present experiments, this viewpoint cannot be ruled out. However, the observable thermal effects in DSC experiments after storage in the poly(ether–ester) copolymers suggest that crystallization on cooling may be the dominant factor in the present case.

The smallest nonzero value of $\langle l \rangle_a$ in Figure 21 for H60/0:100 was achieved by annealing a molded sample in the solid state at 90 °C. The observed contraction on cooling is much smaller than that observed for the sample formed by isothermal crystallization at the same temperature. This indicates that the secondary crystallization processes on cooling will, in general, also exhibit a "path dependence" with respect to the initial treatment[35] and reinforce the notion of "morphology control" of secondary crystallization. The composition dependence observed in Figure 21 is quantitatively less reliable for reasons discussed above. However, the qualitative results are consistent with both intuition and the established morphology/composition dependence (Figures 3–5). For a fixed contraction of the interlamellar spacings, more space is needed in the softer copolymers because of the need to accommodate the polyether diluent excluded from the hard-segment crystallites. Figure 21 also shows that no contractions on storage are observed in H100/0:100 due to the lack of mobility at the storage temperature ($T_g$ = 25 °C).

The qualitative structural considerations presented here (emphasizing morphology control with allowance for fractionation) may have some applicability to previous studies of multiple melting behavior and morphology development in PTMI/PTMO copolymers.[12,31,32] In these studies, the development of a low-temperature "annealing" endotherm during isothermal crystallization (multiple melting) was investigated. This thermal behavior, analogous to that observed in a wide range of semicrystalline materials, may originate according to similar processes which govern secondary crystallization during cooling. As the available space collapses during crystallization, smaller more defective crystals are formed in the amorphous layers due to spatial constraints, and in the copolymers, to the need of accommodating the polyether diluent within the lamellar morphology. In the PTMI/PTMO copolymers, the soft segment acts somewhat "passively" in morphology determination and the crystallization process.[32] This is reinforced in the current work by the observed proportionality of the long spacing with composition and the observation that a larger amorphous layer thickness is required in the softer copolymers to achieve the same contraction of the long spacing during room-temperature storage. In this way, crystallization of the copolymers can be viewed as an extension of the homopolymer crystallization with the additional accounting of fractionation effects and the need to accommodate the soft segment within the semicrystalline microstructure.

**Acknowledgment.** The authors thank Dr. J. Michael McKenna (Polymer Automotive, E.I. du Pont de Nemours & Co.) for synthesis of the polymers used in this

work. Partial funding was provided by the NSF Division of Materials Research (DMR-90-16959).

## References and Notes


(1) Cella, R. J. *J. Polym. Sci. C* **1973**, *42*, 727.
(2) Buck, W. H.; Cella, R. J.; Gladding, E. K.; Wolfe, J. R., Jr. *J. Polym. Sci. C* **1974**, *48*, 47.
(3) Seymour, R. W.; Overton, J. R.; Corley, L. S. *Macromolecules* **1975**, *8*, 331.
(4) Lilaonitkul, A.; Cooper, S. L. *Rubber Chem. Technol.* **1977**, *50*, 1.
(5) Zhu, L.; Wegner, G. *Makromol. Chem.* **1981**, *182*, 3625.
(6) Zhu, L.; Wegner, G.; Bandara, U. *Makromol. Chem.* **1981**, *182*, 3639.
(7) Bandara, U.; Dröscher, M. *Colloid Polym. Sci.* **1983**, *261*, 26.
(8) Vallance, M. A.; Cooper, S. L. *Macromolecules* **1984**, *17*, 1208.
(9) Briber, R. M.; Thomas, E. L. *Polymer* **1985**, *26*, 8.
(10) Briber, R. M.; Thomas, E. L. *Polymer* **1986**, *27*, 66.
(11) Castles, J. L.; Vallance, M. A.; McKenna, J. M.; Cooper, S. L. *J. Polym. Sci., Polym. Phys. Ed.* **1985**, *23*, 2119.
(12) Stevenson, J. C.; Cooper, S. L. *J. Polym. Sci., Polym. Phys. Ed.* **1988**, *26*, 953.
(13) Stevenson, J. C.; Cooper, S. L. *Macromolecules* **1988**, *21*, 1309.
(14) Stockton, W. B. MS Thesis, Princeton University, Princeton, NJ, 1988.
(15) Fakirov, S.; Gogeva, T. *Makromol. Chem.* **1990**, *191*, 603.
(16) Keith, H. D.; Padden, F. J. *J. Appl. Phys.* **1964**, *35*, 1270.
(17) Keith, H. D.; Padden, F. J. *J. Appl. Phys.* **1964**, *35*, 1286.
(18) Keith, H. D. *J. Appl. Phys.* **1964**, *35*, 3115.
(19) Khambatta, F. B.; Warner, F.; Russell, T.; Stein, R. S. *J. Polym. Sci., Polym. Phys. Ed.* **1976**, *14*, 1391.
(20) Warner, F. P.; MacKnight, W. J.; Stein, R. S. *J. Polym. Sci., Polym. Phys. Ed.* **1977**, *15*, 2113.
(21) Alfonso, G. C.; Russell, T. P. *Macromolecules* **1986**, *19*, 1143.
(22) Hahn, B. R.; Hermann-Shonherr, O.; Wendorff, J. J. *Polymer* **1987**, *28*, 201.
(23) Russell, T. P.; Ito, H.; Wignall, G. D. *Macromolecules* **1988**, *21*, 1703.
(24) Kumar, S. K.; Yoon, D. Y. *Macromolecules* **1991**, *24*, 5414.
(25) Helfand, E.; Wasserman, Z. R. In *Developments in Block Copolymers*, Goodman, I., Ed.; Applied Science: London, 1982.
(26) Leibler, L. *Macromolecules* **1980**, *13*, 1602.
(27) DiMarzio, E. A.; Guttman, C. M.; Hoffman, J. D. *Macromolecules* **1980**, *13*, 1194.
(28) Whitmore, M. D.; Noolandi, J. *Makromol. Chem., Macromol. Symp.* **1988**, *16*, 235.
(29) Stevenson, J. C. Ph.D. Thesis, University of Wisconsin—Madison, Madison, WI, 1987.
(30) Gilbert, M.; Hybart, F. J. *Polymer* **1972**, *13*, 327.
(31) Phillips, R. A.; McKenna, J. M.; Cooper, S. L. *J. Polym. Sci., Polym. Phys. Ed.* **1994**, *32*, 791.
(32) Phillips, R. A.; Cooper, S. L. *Polymer* **1994**, *35*, 4146.
(33) Witsiepe, W. K. *Adv. Chem. Ser.* **1973**, *129*, 39.
(34) Richardson, M. J.; Burrington, P. J. *J. Therm. Anal.* **1974**, *6*, 345.
(35) Phillips, R. A. Ph.D. Thesis, University of Wisconsin—Madison, Madison, WI, 1992.
(36) Conix, A.; Van Kerpel, R. *J. Polym. Sci.* **1959**, *XL*, 521.
(37) Bowan, I. J.; Brown, D. S.; Wetton, R. A. *Polymer* **1969**, *10*, 715.
(38) Register, R. A.; Cooper, S. L. *J. Appl. Crystallogr.* **1988**, *21*, 550.
(39) Craven, B. M.; DeTitta, G. T. *J. Chem. Soc. Perkin Trans. 2* **1976**, 814.
(40) Lake, J. A. *Acta Crystallogr.* **1967**, *23*, 191.
(41) Rathje, J.; Ruland, W. *Colloid Polym. Sci.* **1976**, *254*, 358.
(42) Strobl, G. R.; Schneider, M. *J. Polym. Sci., Polym. Phys. Ed.* **1980**, *18*, 1343.
(43) Tanabe, Y.; Strobl, G. R.; Fischer, E. W. *Polymer* **1986**, *27*, 1147.
(44) Vonk, C. G. *Makromol. Chem., Macromol. Symp.* **1988**, *15*, 215.
(45) Robelin-Souffache, E.; Rault, J. *Macromolecules* **1989**, *22*, 3581.
(46) Fakirov, S.; Apostolov, A. A.; Boeske, P.; Zachmann, H. G. *J. Macromol. Sci., Phys.* **1990**, *29*, 379.
(47) Hall, I. J.; Pass, M. G. *Polymer* **1976**, *17*, 807.
(48) Desborough, I. J.; Hall, I. H. *Polymer* **1977**, *18*, 825.
(49) Busfield, W. K.; Blake, C. S. *Polymer* **1980**, *21*, 35.
(50) Bassett, D. C.; Olley, R. H.; Al Raheil, I. A. M. *Polymer* **1988**, *29*, 1745.
(51) Yeh, J. T.; Runt, J. *J. Polym. Sci., Polym. Phys. Ed.* **1989**, *27*, 1543.
(52) Chung, J. S.; Cebe, P. *Polymer* **1992**, *33*, 2325.
(53) Strobl, G. R.; Schneider, M. *J. Polym. Sci., Polym. Phys. Ed.* **1980**, *18*, 1361.
(54) Pope, D. P.; Keller, A. *J. Polym. Sci.* **1976**, *14*, 821.
(55) Schultz, J. M. *J. Polym. Sci., Polym. Phys. Ed.* **1976**, *14*, 2291.
(56) Chung, J. S.; Cebe, P. *Polymer* **1992**, *33*, 2312.
(57) Hsiao, B. S.; Gardner, K. C. H.; Wu, D. Q.; Chu, B. *Polymer* **1993**, *34*, 3986.
(58) Magill, J. H.; Schultz, J. M.; Lin, J. S. *Colloid Polym. Sci.* **1986**, *265*, 193.
(59) Fischer, E. W. *Kolloid Z. Z. Polym.* **1969**, *231*, 458.
(60) Fischer, E. W. *Pure Appl. Chem.* **1972**, *31*, 113.


MA9501914